Accepted, J. Phys. Chem. A, 2022. jp-2021-084273.R2

# Particle Formation from Photo-oxidation of αpinene, Limonene and Myrcene

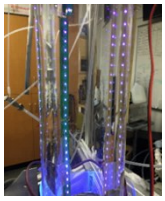

*David R. Hanson*, Adam Sawyer, Darlene Long, Dominick Sofio, Joan Kunz, Michael Wentzel*

Department of Chemistry, Augsburg University, Minneapolis, Minnesota, 55454

* hansondr@augsburg.edu, ph: 612-330-1620

ABSTRACT We present measurements of the effect of first-generation secondary organic aerosol (SOA) material on the growth of ~10 nanometer diameter seed particles composed of sulfuric acid and water. Experiments were performed in an atmospheric pressure, vertically-aligned flow reactor where OH was produced from HONO photolysis in the presence of either $SO_2$ or a monoterpene. For typical conditions, organic compounds at ~300 ppbv are exposed to photo-oxidation for a time of ~80 s at an [OH] of about $6x10^6$ $cm^{-3}$: thus oxidation products have minimal OH exposure. The measured size changes of the sulfuric acid seed particles can then be attributed to uptake of first-generation products. Along with descriptions of the apparatus and the procedure, the analysis to obtain SOA yields by comparing to growth with $H_2SO_4$(g) is detailed. Results from photo-oxidation experiments of αpinene, limonene and myrcene give SOA yields of 0.040, 0.084 and 0.16, respectively. These SOA yields roughly double with each addition of a double bond to the compound. The αpinene and limonene results are in accord with the results of many previous SOA experiments while the myrcene SOA yield stands alone. Photo-oxidation of myrcene also led to significant nucleation and the species responsible is comparable to $H_2SO_4$ at 35 % relative humidity in its nucleation capability.

## INTRODUCTION

Nanoparticles in the atmosphere have significant effects in the climate system and they can detrimentally affect human health. Nucleation and growth of particles important in the atmosphere has focused on agents such as $H_2SO_4$ and oxidized organic compounds, both undergoing intense scrutiny over the decades. The focus of this study is the nucleation and growth of nanoparticles from the photo-oxidation (i.e. OH-initiated oxidation) of αpinene, limonene and myrcene. These processes were studied in a new photolysis apparatus, a growth flow reactor, which is fully presented here.

Previous work[1-4] shows that large amounts of oxidized organics can accumulate on particles (so-called secondary organic aerosol, SOA) and that new particles can be formed, particularly when ozone is the initiating oxidant. There is a wide range in laboratory yields, the fraction of reacted monoterpenes that end up on particles, from a few percent to over 50 % (e.g. 5-14 and references therein). Any number of experimental details influence the measured yield. Yields have been determined by directly monitoring particle sizes and they have also been inferred from measured concentrations of low-volatility products. SOA is produced whether the oxidant is ozone or OH, and whether or not NO is present. While these details are important and influence the measured SOA yields, it appears that experiments with long oxidation times and depletion of the monoterpene report the highest yields. These high yields may then be due to the further oxidation of the monoterpene oxidation products. Considering the evolution of the volatility of the SOA material has led to a better understanding of SOA yields and how they change with time and other experimental conditons.[15-17] Work focusing on the quantification of highly-oxidized molecules (HOMs)[18-21] generally report low[13] yields for first-generation HOMs compared to SOA yields but detection sensitivities are uncertain. Recent work on quantifying the processes responsible for these HOMs shows that rapid oxidation can take place for some peroxy radicals and that dimerization of them may be efficient leading to essentially involatile SOA species.[22-26] New studies directed at measuring SOA produced from only first-generation products of the photo-oxidation of monoterpenes can provide important information for confirming and/or discerning the dominant chemistry that leads to strongly-sticking SOA material.

In an approach similar to that recently demonstrated[13] for αpinene ozonolysis, a flow reactor operated at moderate oxidation rates, we performed SOA growth experiments in an atmospheric pressure flow reactor where OH was produced from HONO photolysis at moderate rates. This new Growth Flow Reactor, GroFR, is based on our[27,28] recently developed Photolytic Flow Reactor (PhoFR) where $H_2SO_4$, from the photooxidation of $SO_2$, formed and grew new particles. OH exposures and overall oxidation rates in the GroFR are generally lower than those in other oxidation flow reactors (e.g. ref. 29). The model[27,28] used to understand growth in the PhoFR was also used here to quantify GroFR monoterpene photo-oxidation experiments. This model was used to (i) provide chain lengths needed to estimate SOA molar yields from measured particle growth and (ii) to identify oxidation products that could be responsible for this SOA.

Photo-oxidation studies in a flow reactor have short reaction times and the SOA material can have small exposures to OH, here the product [OH]**t* is typically $5x10^8$ $cm^{-3}$ s. The flow reactor is operated under laminar flow conditions where the chemical kinetics can be modeled in two dimensions (axial-symmetric), as was done for PhoFR[27,28]. A high level of cleanliness is important as impurities may affect how SOA material is taken up by seed particles but most importantly if homogeneous nucleation from SOA molecules occurs.

In experiments performed in the absence of sulfuric acid seed particles, nucleation of particles in the photo-oxidation of limonene and myrcene was observed. These results are presented along with a comparison to nucleation from $H_2SO_4$ from $SO_2$ photo-oxidation. Finally, the reaction of αpinene with $O_3$ (without an OH scavenger) was studied and from the results of a few experiments, an SOA yield for particle growth was estimated.

## EXPERIMENT

The glass flow reactor, Figure 1, is vertically aligned, ~120 cm in length and has a 5.0 cm inner diameter. Most of its length is enclosed by a cooling jacket through which thermo-stated water flows, maintaining a temperature of 296 K. The main gas flow of 1.55 standard L $min^{-1}$ (sLpm, for standard conditions of 273 K and 1 atm) is composed of air purified by a pressure-swing adsorbent device (AADCO 730). The flow reactor pressure is kept slightly above (+0.001 atm) ambient pressure (~0.97 atm) and relative humidity is 35 (+/-3) %, set by sending a metered portion of the flow (0.5 to 0.6 sLpm) through a humidifier. Table 1 compiles experimental details and typical conditions. The flow reactor wall was cleaned a few years ago but has not been since and on its surface is probably aqueous sulfuric acid residue; a small flow of humidified clean air is maintained through GroFR while not in use.

Particles were sized with a mobility particle sizer (custom 5 μCi Am-241 charger, coupled to a TSI3085 nano-DMA, closed/recirculating sheath flow), amplified with an ultrafine condensation particle counter (diethylene glycol (DEG) vapor) and detected with a butanol condensation counter (TSI3760).[27,30,31] This DEG system has a sampling flow rate of ~2.2 L $min^{-1}$ thus a makeup flow of 0.7 sLpm was added near the sampling port at the bottom of the flow reactor.

$H_2SO_4$ seed particles were produced by sending a small flow (0.03-0.05 sLpm) over a warmed (50 to 60 $^0$C) 96 % $H_2SO_4$ solution and mixing this with a ~0.5 sLpm flow of moist air. After entrainment and mixing with the ~1.0 sLpm main dry flow plus the HONO-containing flow, seed particle number densities were typically 3-to-10$x10^3$ $cm^{-3}$. The size distributions had a leading edge that was well-described by a log-normal function with typical mode diameters 8-to-10 nm and lnσ of 0.13-to-0.16. At a relative humidity of 35 %, a bulk sulfuric acid solution would contain 50 % $H_2SO_4$ by weight and have a density of 1.39 g $cm^{-3}$.[32] These bulk properties are nearly attained by a 10 nm diameter sulfuric acid particle: calculations[33,27] show they are about 54 wt %.

Photo-oxidant HONO was prepared by reacting HCl(g) with NaONO(s),[34] as in our previous photolytic work[27,28], with a few changes detailed here. The aqueous HCl reservoir generated about 7 μmol/mol (ppmv) HCl and water vapor at about 85 % humidity (4 mol NaCl and 2 mol $H_2SO_4$ per kg water[32]); the reservoir was at room temperature which was fairly steady at 22±2 °C. The small (5 mL) vessel holding the NaONO powder was held at 70 to 80 $^0$C. The levels of $NO_{x'}$ (here HONO+NO+$NO_2$ and perhaps ClNO[35]) and NO were periodically checked using a calibrated NO chemiluminescence detector (TECO 42/b). For a typical flow from the HCl reservoir, $Q_H$, of 0.010 sLpm, the NOx' (HONO) mixing ratio in the flow reactor was 45 (42) nmol/mol (ppbv) and initial NO and $NO_2$ were each 1.6 ppbv. Note that a flow of 0.04 to 0.2 sLpm of dry air was also sent over the NaONO(s) which flushed the 5 mL vessel, as suggested by Febo et al.[34] HONO and NO levels were not dependent on flush flows of 0.04 sLpm or larger. Without a flush flow, impurity NO levels as high as 10 % of the NOx' level were observed. The flush flow also kept HCl below 4 ppmv in the vessel, a threshold level that inhibits ClNO formation.[35] We assume $NO_2$ is present at the same level as NO. The supplement presents chemiluminescence measurements supporting this assumption.

HONO was photolyzed with ultraviolet LEDs (Vishay Semiconductors, peak emission 365 nm) strung into two banks of 108 LEDs that each extend over a length of ~100 cm of the reactor. The banks point to the center of the reactor and are situated at roughly 90$^0$ angles. Illumination level is determined from the total current, $I_{LEDs}$, through the LED assemblies: full illumination is 2.0 A (1.0 A for each bank); in practice, $I_{LEDs}$ was generally maintained between 1.9 and 2 A. Full illumination is a current of 28 mA for each LED with each bank having 36 sets of three LEDs in series. $I_{LEDs}$ was controlled by a voltage of between 10 and 12 V applied across each set of three LEDs and a current limiting resistor. At full illumination the photolysis rate of HONO was estimated to be 0.0020 $s^{-1}$ (see Results below).

A monoterpene, either αpinene, limonene, or myrcene (used as is from Sigma-Aldrich with purities of 98%, 95% and >75%, respectively), was introduced via a small flow (0.6 mL/min) over a liquid aliquot held in a small vessel immersed in an ice bath. The 273 K vapor pressures[36] are 0.5 mbar for limonene[38] and myrcene[38] and 1 mbar for αpinene[37] and after dilution in the main flow the monoterpene level in the flow reactor was 200-400 ppbv: note that

particle growth results did not depend on the carrier flow (from 0.4 to 6 sccm) providing evidence that the monoterpene level was high enough that oxidation products did not significantly interact with OH (see Supplement). $SO_2$ could be introduced from a dilute mixture in nitrogen (ranging from 1 to 10 %) and it was typically present at a few ppmv for the $H_2SO_4$ growth calibration experiments.

Figure 1. Schematic of apparatus. Top port was used for a few ozonolysis experiments.

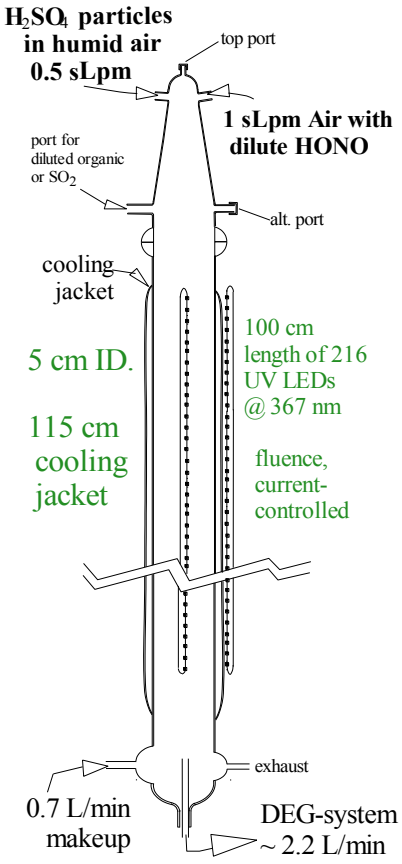


Our experimental approach relies on growth experiments with $H_2SO_4$ to provide a standard for quantifying SOA yields for the same photo-oxidation conditions. Our analysis focuses on condensable species where the flow reactor wall is the dominant sink: typical first-order loss rate coefficients in our experiment are ~$3x10^{-2}$ $s^{-1}$ to the wall and ~$3x10^{-5}$ $s^{-1}$ to seed particles. Semi-volatile species might not have a sustained loss to the wall and in that case 0.012 $s^{-1}$, the inverse of the 85 s average residence time in the flow reactor, is the dominant loss process. The details of relating a particle's observed growth to its $H_2SO_4$ exposure is presented in our previous study (ref. 28, sections 3.2, 3.3 and S3).

When comparing growth from photo-oxidation of $SO_2$ to growth from photo-oxidation of an organic species, the differences in the gas-phase chemistry must be considered. In particular, the regeneration of OH from $HO_2$ + NO can lead to more oxidation of $SO_2$ than a monoterpene would undergo because in the latter NO reacts first with $RO_2$ radicals. Furthermore, $HO_2$ production is delayed and $HO_2$ also can react with $RO_2$ in the monoterpene cases. The SOA was assumed to have a density of 1.2 g/mL, a molar mass of 210 g/mol (e.g. ref. 13) and the water content of the seed particles was assumed to be constant. The main factor in extracting the SOA yield from the measurements is OH regeneration in the $SO_2$ experiments: OH regeneration in the organic experiments is weak and not dependent on the details of the chemistry.

A two-dimensional (2D) model of the photolytic flow reactor,[27,28] was adapted to include the chemistry of the OH-initiated oxidation of αpinene, a chemistry that is not fully known and even the established pathways are not known to be substantively complete. Nevertheless, we used the chemistry in the Master Chemical Mechanism, MCM v3.2[40] (via website: http://mcm.leeds.ac.uk/MCM) and also incorporated are the recent rates and pathways for

the H-shift reactions (McVay et al.[8]; Xu et al.[25]; Zhao et al.[24]; Berndt et al.[23]) The suggested 40% yield pathways of Vereecken et al.[39] regarding the alkoxy radicals formed in the NO reactions with APINBO2[40] and APINAO2[40] were retained but at only 4 % yields. The $SO_2$ and the inorganic chemistry were developed previously[27,28] and $SO_2$ level can be set to zero so that αpinene photo-oxidation occurs with the inorganic photo-chemistry module. Details of the chemistry are presented in the supplement. The inorganic module now includes the photolysis of $NO_2$ that produces NO and ozone and ozone reactions with NO, OH and $HO_2$ as well as the ozone + monoterpene reaction. These adaptions and modifications are detailed in the supplement.

## RESULTS

### *Growth of sulfuric acid – water seed particles*

Changes in particle size for a typical growth experiment is depicted in Figure 2 where six size distributions are shown: two with LEDs off and four with the LEDs on. Experiments with two HONO levels are shown, $Q_H$=15 and 36 sccm, and αpinene was 400 ppbv; note that adding them to the gas caused no significant change in the seed particle distributions. The data in Fig. 2 show that the change in the distributions are repeatable for back-to-back LED on–off cycles. The shape of the primary mode in the leading edge remains log-normal upon photo-oxidation and the change in size is robust for constant HONO and NO content. Note that there are variations day-to-day of up to 20 % in HONO and NO for a given flow $Q_H$ (see Supplement.)

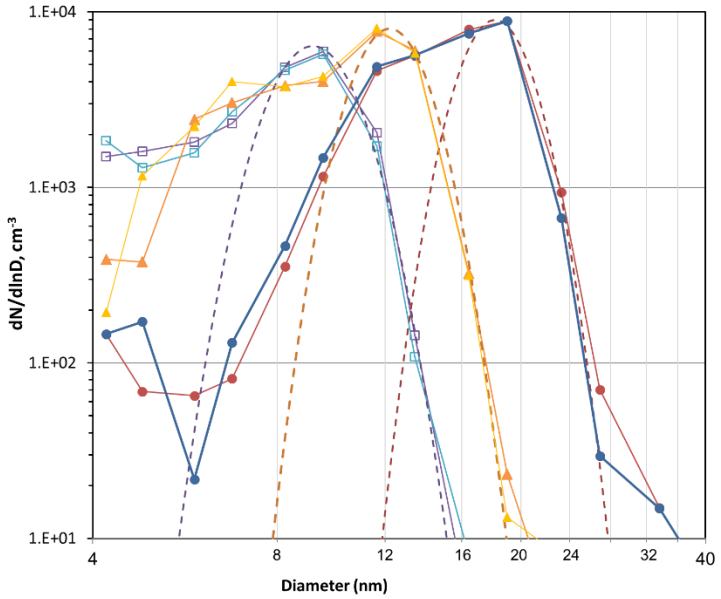


Figure 2. Change in diameter of seed particles due to photooxidation of pinene. Open squares are LEDs off, others are LEDs on at 2 A: triangles QH=15, circles QH=36. The log-normal distributions fitted manually to the leading edge of the particles are also shown (ranges: maximum from 6400 to 9000 cm-3, mode diameter from 9.2 to 18.2 nm, and ln from 0.14 to 0.115).

The size distributions show the presence of particles not in the main log-normal mode. They are smaller and fewer than the main mode and are not likely to affect the overall growth conditions in the reactor. Their apparent increase in size is consistent with the behavior of the main mode and their increase in number could be due to better transmission down the flow reactor as they grow. For some conditions significant nucleation occurred, e.g. myrcene photo-oxidation experiments at high oxidation rates, and a prominent mode at small sizes appears. More on that in the nucleation section below. Interestingly, the seed particles grew by about 1 nm for $Q_H \geq 5$ sccm in the absence of an organic. When octane or isoprene were present this growth essentially disappeared; these data are shown in the Supplement. These findings suggest that the high levels of OH in the absence of an organic oxidizes something in the seed particles, perhaps bisulfate leading to persulfate species.

Shown in Figure 3 are the change in particle diameter due to photo-oxidation of myrcene as $I_{LEDs}$ was varied. The linear regression indicates that there is a close-to-linear dependence of the change in particle size with photo-oxidation rate. The three data points near full illumination (1.6 to 1.9 A) are not included in the regression because significant nucleation occurred for these conditions, partially obscuring the leading edge of the distribution. Since these three data points are well within the scatter of the measurements (Figure 4), their modest divergence from a

linear relationship at large oxidation rates is not considered significant. For the myrcene SOA growth experiments, HONO levels were kept at or below $Q_H$=0.010 sLpm to avoid large numbers of small particles.

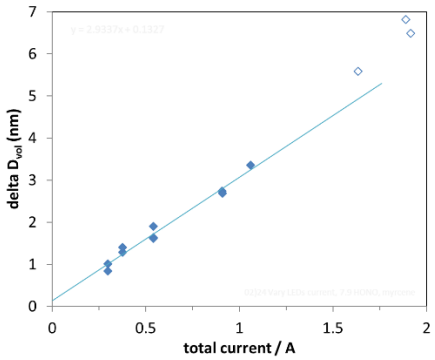


Figure 3. Diameter change with LED illumination. Myrcene with 32 ppbv HONO present. At 1.6 A and above there was significant nucleation and points are indicated as open diamonds. A linear regression for data up to 1.1 A is shown. The y-axis is the change in the volume-weighted mean diameter.

Figure 4 is a summary plot of the change in particle diameter ($D_{vol}$, volume-weighted average diameter) for the three monoterpenes as a function of $Q_H$, the flow through the HCl reservoir. Full illumination was used for all data which was taken over a three-month period in early 2021. The change in diameter was calculated from the volume mean diameter of the size distributions. There is significant scatter which is due to variations in HONO and NO at a given $Q_H$ and other factors such as changes in flow patterns in the reactor and in how the makeup flow affects the sampling of the main flow.

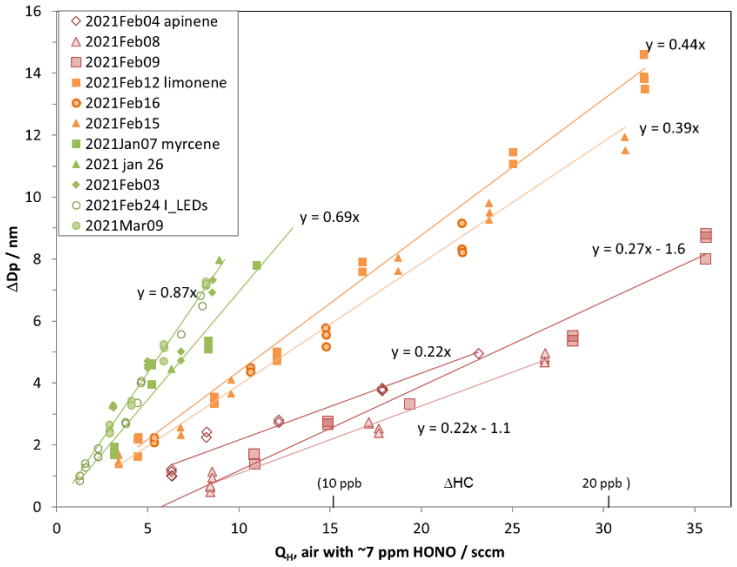


Figure 4. Change in diameter due to photooxidation of monoterpenes vs. flow rate of ~7 ppmv HONO-in-air mixture. SOA yield increases from □pinene (red symbols) to limonene (orange symbols) and then myrcene (green). The data is primarily with ILEDs of 1.9 to 2 A except for the open circles for myrcene data (from Fig. 3) which are plotted as QH×1.92A/ILEDs. Linear fits forced through zero describe the myrcene and limonene data while the scatter in the □pinene results leaves the dependence open for discussion. The amount of □pinene, □HC, reacted along the length of the flow reactor was calculated with the 2D-model and ticks are plotted for 10 and 20 ppb.

Growth is approximately linear with the amount of HONO initiator present for all three monoterpenes. The photo-oxidation of myrcene (3 double bonds) leads to the largest growth in the seed particles followed by limonene (2 double bonds) with αpinene (1 double bond) trailing. These observations suggest that the concentrations of particle-growth products scales linearly with oxidation rate: here, HONO level at constant $I_{LEDs}$. Note the results shown in Fig. 3 are also plotted in Fig. 4 as the open green circles, normalized to 1.92 A.

*Analysis for obtaining SOA yields*

Experimental SOA yields on a mole basis were estimated from the changes in diameter in Fig. 4 and comparing them to the diameter changes in the $SO_2$ growth experiments that were conducted under similar conditions (seed particles, HONO abundances) but at reduced LED current, $I_{LEDs}$. Results from two experiments at $I_{LEDs}$ = 0.45 and 0.25 A are shown in the Supplement where growth closely follows a linear relationship with slopes given by $I_{LEDs}\times 5$ (nm /sccm / A). Lower photolysis rates were used in the $SO_2$ experiments to limit growth rates because $H_2SO_4$ is formed at 100 % yield. To obtain an SOA yield from the ratio of the growth slopes for organic photo-oxidation to $SO_2$ photo-oxidation: (i) the kinetics of the uptake of $H_2SO_4$ (SA) differ from that of SOA molecules, (ii) the volume properties for the two materials differ, and (iii) the chain length for regeneration of OH molecules, $f_{CL}$, can be much larger for $SO_2$ photo-oxidation than for photo-oxidation of an organic species.

We consider those three factors for the case where uptake onto small particles is not limited by gas-phase diffusion and relative humidity is constant. The growth rate, $dD_p/dt$, of a particle of diameter $D_p$ due to uptake of vapor species *v* with uptake coefficient γ is given by[41,42,28]

$$\frac{dD_p}{dt} = \frac{k_{GR}[v^*]}{\left(1+\frac{D_p}{3}\frac{\partial \ln(w\rho)}{\partial D_p}\right)} \qquad \text{Eq 1a.} \qquad\qquad k_{GR} = \frac{M_v \gamma \overline{c_r}}{N_A 2 w \rho}\left(1+\frac{d_{v*}}{D_p}\right)^2 \qquad \text{Eq 1b.}$$

The * designation on *v* indicates hydration of the *v* molecule, [v*] is the number density of this vapor species summed over all hydrates, $M_v$ is *v*'s molar mass, $N_A$ is Avagadro's number, $\overline{c_r}$ is the mean molecular speed for the reduced mass of the particle – *v** (using the average hydrate mass) encounter, $d_{v*}$ is the diameter of the average hydrate vapor species, *w* is the weight fraction of *v* in the particle and ρ is the density of the particle. The term in the denominator in Eq 1(a) accounts for changes in *w* and ρ with particle size, a swelling-with-size factor. For sulfuric acid particles of 10 to 17 nm diameter, this term has a value of 0.97-to-0.975 for 35 % RH and 296 K. The value of this term is not known for SOA material (or whether SOA may affect the properties of sulfuric acid) but it is likely to be of this order and the difference in this term between SA and SOA molecules is considered to be negligible. Not needed here is a swelling-with-humidity term.[28]

Enhanced uptake due to van der Waals forces is assumed to be insignificant here. The Stolzenburg et al.[43] analysis indicating there is a van der Waals enhancement of uptake for $H_2SO_4$ depends on which model was used to calculate how much water was lost upon sampling the 2-to-8 nm diameter particles. These models need rigorous experimental verification.

The rate of change of diameter (Eq 1) is directly related to the concentration of the condensing vapor [v*] and below we directly apply Eq. 1 to estimate a diameter change from model-calculated concentrations. Here we obtain an estimate for the number density of SOA molecules, and thereby an SOA yield, produced from monoterpene photo-oxidation by comparing growth rates with those for $SO_2$ photo-oxidation. The ratio of Eq. 1 for SOA (where [SOA]=[v*]) to Eq. 1 for $SO_2$ (where v = SA has a 100% yield and uptake is unity[44]) allows one to estimate an SOA yield, with a few assumptions about the SOA molecules. (1) SOA material is produced at a rate = $Y_{SOA}k_{phox,org}$ where $Y_{SOA}$ is the molar yield from the organic and $k_{phox,org}$ is the rate at which the organic species is photo-oxidized. (2) Its major loss process is to the wall with no re-evaporation, i.e., it is considered non-volatile. (3) SOA material is assumed to have a molar mass of 210 g/mol and a density of 1.2 g/cm$^3$. If particle-phase chemistry between organic species is significant, these assumptions may need to be revised. See the Supplement for further discussion of particle-phase chemistry.

The molar yield of SOA is obtained from the slope of the growth data, $m_{SOA}$, scaled to that from the SA growth data, $m_{SA}$, along with kinetic and volume properties using the following equation:

$$Y_{SOA} = \frac{D_{SOA}}{D_{SA}} f_{CL} \frac{c_{SA}}{c_{SOA}} \frac{V_{SA}}{V_{SOA}} \frac{m_{SOA}}{m_{SA}} \qquad \text{Eq 2}$$

The ratio of diffusion coefficients[45,46] (0.74) takes into account differing loss rates to the wall. The chain length factor ($f_{CL}$ = 2.9) accounts for differences in how much $SO_2$ reacts compared to how much monoterpene reacts for identical photolysis conditions ($k_{phox,SA}$ vs. $k_{phox,org.}$) The ratio of mean molecular speeds (1.25) is a kinetic factor (accounting for hydration of SA[45]) and the ratio of molar volumes for SA vs. that assumed for SOA (0.75) is accounted for as well. See the Supplement for the derivation of Eq 2 and for the details in how values for these quantities were estimated.

The chain length factor varies only slightly with the choice of organic species: we ran a cyclohexane scheme[47] in place of the αpinene scheme and obtained a factor of 2.6 for $f_{CL}$. Also, $f_{CL}$ depends on the level of NO entering the flow reactor and to a lesser extent on $I_{LEDs}$, see the Supplement. Finally, a HONO photolysis rate of $2.5\text{x}10^{-4}$ s$^{-1}$ was needed for the model to match the observed growth in the $SO_2$ experiments ($I_{LED}$ = 0.25 A.) This translates into a photolysis rate of $2.0\text{x}10^{-3}$ s$^{-1}$ for full illumination (2 A.)

In practice, the SA growth slopes were performed at reduced $I_{LEDs}$ because growth is so effective in $SO_2$ photo-oxidation. Then an additional factor, the ratio of LED currents, is included in the $Y_{SOA}$ calculation. The monoterpene oxidation SOA yields are given approximately by the slope $m_{SOA}$ from Fig. 4 divided by $m_{SA} = 5 \times I_{LEDs} = 10$ (nm / sccm / A) and multiplied by the factors discussed above:

$$Y_{SOA} = 2.0 * m_{SOA} / (5 \cdot I_{LEDs} \text{ nm sccm}^{-1} \text{ A}^{-1}) = 0.40 \; m_{SOA}/I_{LEDs} /(\text{A nm sccm}^{-1}) \qquad \text{Eq. 3}$$

For the monoterpene experiments $I_{LEDs} = 2$ A and the SOA yield is equal to $0.20 \cdot m_{SOA}$. From the slopes in Fig. 4 -- 0.20, 0.42 and 0.78 -- the SOA molar yields are 0.040 for αpinene, 0.084 for limonene, and 0.16 for myrcene. These are uncertain to +/- 40 %, which is the estimated uncertainty in the factor $f_{CL}$ coupled with the assumptions above.

*Model calculated gas-phase concentrations*

Alternatively, gas-phase concentrations predicted in the 2D-model can be used along with Eq.1 to estimate diameter changes assuming efficient uptake. Attributing the growth to particular species is the second and more uncertain way the model results are used here. The model for the photo-oxidation of αpinene was run for experimental conditions of 400 ppbv αpinene and $Q_H = 10$ sccm resulting in a simulated loss for αpinene of 6 ppbv over the length of the reactor (detailed results below). The model is focused on the OH addition channels but contains placeholders for: (i) OH abstraction, (ii) reaction with ozone that is generated from the photolysis of $NO_2$, and (iii) the reaction of OH with the major gas-phase product, pinonaldehyde. For these conditions, OH abstraction products had a 11.6 % yield, the ozone product placeholder 0.3 % and the OH plus pinonaldehyde tracer product had a yield of 0.16 %. There is very little OH chemistry beyond reaction with the monoterpene in the experiment.

Model results for seven gas-phase products of αpinene photo-oxidation are presented in Figure 5, a plot of the on-axis (R=0) concentrations as a function of Z (axial distance). These first-generation (loosely defined as arising from one OH reaction) products of the OH addition channels are the most abundant initial peroxy radical (black dashed) and six representative stable species: sum of multifunctional-nitrates with up to 6 O atoms (orange), sum of the hydroxy-hydroperoxides (yellow, from $HO_2$ + peroxies, rate coefficient of $2 \times 10^{-11}$ $cm^3$ $s^{-1}$), the 8-OOH-menthene-6-one species (blue, Vereecken et al.[39] also Berndt et al.[50]), two sums of the $RO_2$+R'$O_2$ dimers (green, formed from peroxy radicals with less than 7 O atoms and red, formed from HOPs, highly-oxidized peroxy radicals, $C_{10}H_{17}O_7$), and finally the nitrate products of the reactions of these HOP radicals with NO (brown). All species except en-one-OOH were reacted with the wall, limited by diffusion. The HOPs in the model are species 19, 20, and 29 of Berndt et al.[50] ; we assume that the cyclization that produces them dominates over the alternate pathway, the 1,6-H-shift. The Supplement has plots of the HOPs and other radicals as well as the inorganic species for these conditions.

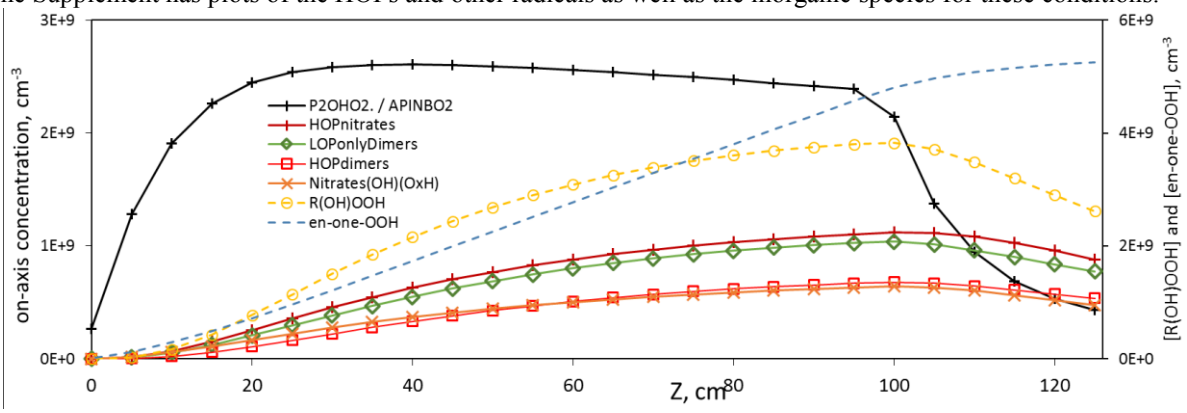


Figure 5. On-axis gas-phase concentrations of selected products from modeled □pinene photo-oxidation. These OH–addition representative products are: an initial peroxy, APINBO2 = P2OHOO· (black); sum of all hydroxy-hydroperoxides, R(OH)OOH (yellow, right axis); 8-OOH-menthene-6-one, en-one-OOH (blue, right axis); two sums of products of the four highly-oxidized peroxies in the APINCO2 scheme (HOPs = C10H17O7·) - the HOPdimers (red) and 30% of the products of NO reactions with HOPs, HOPnitrates (brown); sum of the three-functional-group nitrates, Nitrates(OH)(O1,2H) (orange); and the sum of dimers from less-oxygenated peroxy radicals (green). All species except en-one-OOH are lost on the wall at the diffusion limit.

We can estimate particle growth from these model results by applying Eq. 1 with an exposure time of 42 s (see the supplement for evidence that supports using the on-axis concentrations and residence time). For these conditions, the observed particle growth was roughly 2 nm. The average concentration of the peroxy radical leads to a diameter increase of 2.2 nm, if taken up efficiently and the next most abundant $RO_2$ (APINAO2, not shown) could contribute 1.1 nm (see the Discussion where heterogenous reactions of these radicals are considered). The

dihydroxy- and (OH)(OOH)-nitrates have the ability to increase the diameter by ~ 0.5 nm and 0.8 nm, respectively. The multitude of R(OH)OOH species (yellow) and the en-one-OOH[39] species (species 16 in Berndt et al.[50]) have the potential to change the diameter by 2.7 nm and 3.1 nm, respectively, but these species have relatively high volatilities[67]. The low-oxygen content dimers (LOP, green) could result in a diameter change of 1.0 nm while the high-oxygen content dimers (HOP, red) could increase particle diameters by 0.6 nm (assuming molar masses of 400 g/mole). The highly-oxidized peroxies (HOPs) are formed at a significant rate but their abundance is low due to their reaction with NO yet the nitrate products of these NO reactions (assumed 30% yield) together could grow the particles by 0.8 nm. For the present experimental conditions and assumed H-shift rate coefficients, there is a large role for the chemistry of these HOP species.

The model indicates there are many multifunctional products that have sufficient gas-phase abundances to affect particle sizes, depending on their volatility. While those with only two functional groups are likely too volatile to effectively influence particle size, those with three functional groups might have low enough vapor pressures (e.g. ref. 15, 48, 67) to participate in building SOA mass. For example, the dihydroxy- and (OH)(OOH)-nitrates and particularly the HOPnitrates - (OH)(OOH)($NO_3$) with a peroxide bridge - might have sufficiently low vapor pressures[48] that a significant amount may be taken up by particles (mole fractions in the organic phase of the aerosol of 0.1 to 0.3). See Table 2 for a list of equilibrium particle phase partitioning for a range of semi-volatile species.

Undoubtably, the dimers are of very low volatility[49,50], and it is likely they would efficiently grow the seed particles. However, the model results were obtained using a 100 % yield and rate coefficients for the $RO_2$ self-reactions that range from 2-to-20x$10^{-12}$ $cm^3$ $s^{-1}$. We followed Schervish and Donahue[49] for the dimerization rate coefficient dependence on the number of O atoms in the $RO_2$'s. They also propose that the yield of the dimer depends on the oxidation state of the $RO_2$'s and a value of 0.1 would apply for the most oxidized peroxies that were simulated here. If these low yields better describe the chemistry, the model suggests the dimer concentrations would plummet accordingly and the majority of the observed particle growth would have to be attributed to non-dimer species. Note that knowledge about the rates and dimer yields of the highly-oxidized peroxies is fluid at the moment: Berndt et al.[23] suggest a large rate and a high yield for the dimer while Zhao et al.[24] suggest much lower rates (factor of ten) and yields of ~0.04.

*Limonene SOA volatility*

Burkholder et al.[14] studied particle growth in OH and ozone αpinene oxidation and they quote upper limits to the 298 K vapor pressures of condensing substances of 20 ppt or ~5x$10^8$ $cm^{-3}$. This abundance is attained by many species in our model simulations and particularly the multifunctional nitrates could condense as they presumably have low volatilities (Valorso et al.[48] report a range of estimation methods.) To experimentally test the volatility of the SOA material, we sent the aerosol through a heated 30 cm long ½" OD copper tube placed before the DEG system; one set of experiments for limonene is depicted in the supplement. The setup also acts to denude the aerosol sample as it undergoes cooling along a room-temperature 60 cm length of copper tubing before entering the DEG system and any remaining degassed species are lost to the wall. When the 10 nm diameter seed particles were sent through the copper tube heated to 120 $^0$C, they shrank to ~ 4 nm in diameter whereas with a limonene SOA coating of ~ 2 nm, the 12.2 nm diameter particles shrank to ~ 9 nm. The residence time in the heated section is only about 1 s so volatility cannot be quantified[51,52], yet these observations suggest that the SOA material has a vapor pressure less than ~2x$10^{-5}$ atm at 120 $^0$C, the partial pressure of $H_2SO_4$ over a 90 wt% sulfuric acid solution at 120 $^0$C and a water partial pressure of 0.01 atm[53,54]. Note that the SOA material may undergo additional reactions as it is heated[52] diminishing the estimate of the SOA vapor pressure.

*Nucleation from OH plus myrcene and limonene*

As noted above, myrcene photo-oxidation led to significant homogeneous nucleation for the present experimental conditions. Plotted in Figure 6 are the results of measurements varying $Q_H$ without seed particles with $I_{LEDs}$ = 2 A; also shown are results for $SO_2$ with $I_{LEDs}$ varying from 0.08 to 1 A at $Q_H$=7.5 sccm. The x-axis is plotted as $Q_H$ * $I_{LEDs}$ / 2 A for better comparison of the results at *initial* OH production rates (i.e., HONO photolysis rates): keep in mind that additional OH is produced from $HO_2$ + NO which is most active for $SO_2$ (the $f_{CL}$ factor). The size distributions (see the Supplement) were spread out across a range of diameters but a leading edge mode can be identified and what is plotted on the y-axis are the number in this mode which can be represented by a log-normal function. The particle mode diameters are indicated for a few data points. For equivalent photo-oxidation conditions, the nucleated particles attained sizes that are about 70 % of the diameter change that seed particles underwent. This is probably due to decreased exposures to SOA material for nucleated particles because they are formed well into the illuminated section while seed particles have the entire length of the illuminated region to accumulate material.

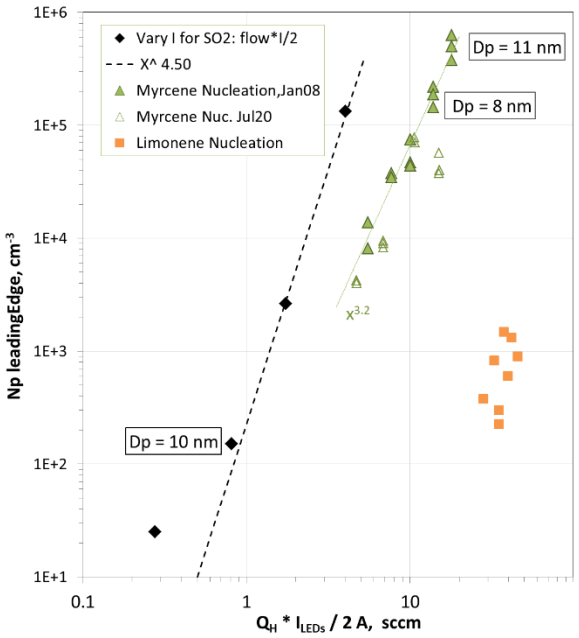


Figure 6. Nucleation in photo-oxidation of myrcene (green) and limonene (orange) with ILEDs = 2 A. Black diamonds are nucleation from H2SO4 produced from SO2 with QH= 7.7 sccm and ILEDs varying from 0.07 to 1.0 A. Number of particles are plotted vs. QH, flow rate through HONO source (for SO2, normalized to ILEDs). The myrcene Jul20 (2021) experiments had 10 ppm HCl content in QH and thus data is plotted as QH×10/7.

Photo-oxidation of myrcene is a prodigious source of new particles, comparable to $H_2SO_4$ at 35 % RH formed in $SO_2$ photo-oxidation. We compare the data that produced ~ 10 nm diameter particles (see the data point callouts). As a first try at comparing these data, we assume that the growth species is the nucleating species for myrcene as it is for sulfuric acid. Thus the abundance of the nucleating species is similar for these two data points (the larger $V_m$ for myrcene than for SA suggests that [v*] for myrcene could be smaller than [SA]). The myrcene nucleating species leads to a number density of particles that is three orders of magnitude larger than the number density of particles produced at a comparable (or probably larger) abundance of $H_2SO_4$. Note that the myrcene photooxidation nucleating species may be just a fraction of the 15 % SOA growth yield from myrcene, furthering the nucleation capabilities of this species over that by $H_2SO_4$ at 35 % RH and 296 K.

The nucleation of particles from αpinene photo-oxidation was non-existent for all conditions while it was measurable for limonene but significantly less than myrcene exhibited. The limonene nucleation data are shown in Fig. 6 as orange squares. The $N_p$ generated with limonene was much lower than that for the myrcene experiments while the size of the nucleated particles was similar to those formed in the myrcene nucleation experiments, ranging from 5 to 10 nm in diameter. Interestingly, the equivalent growth capabilities for limonene to change the seed particle diameters by 5 to 10 nm (see Fig. 4) occurred for oxidation rates (i.e, $Q_H$) of 45 % of those in the nucleation measurements. This is consistent with the supposition inferred from the myrcene results that nucleation occurs well into the illuminated section of the flow reactor.

*Ozone plus αpinene: Growth and nucleation.*

A final set of experiments demonstrating the apparatus and its capabilities are particle growth measurements due αpinene ozonolysis. Figure 7 shows the results of ozone plus αpinene runs where ozone was held constant at 230 ppbv produced with a hard UV (185 and 254 nm) mercury lamp, monitored with a Dasibi 1003, while the flow of air over the αpinene liquid at 0 $^0$C, $Q_{org}$, was varied. The size of the seed particles is indicated at $Q_{org}$ = 0 which was not subtracted from the growth data as it was for the photo-oxidation experiments; two runs with different number densities of seed particles were performed and the results are nearly identical. No compounds were added to act as OH scavengers.

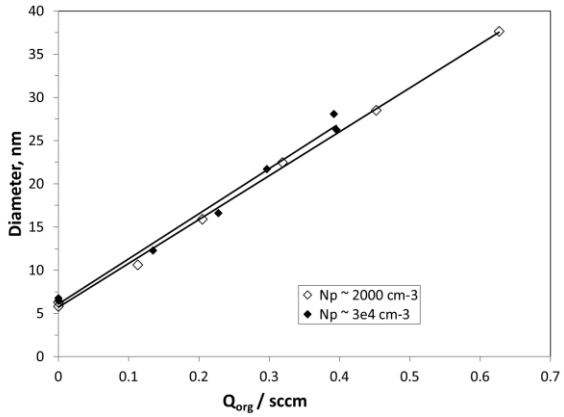


Figure 7. Growth of seed particles due to ozonolysis of □pinene. There was 230 ppb O3 present and growth experiments at two different number densities of seed particles were performed. Flow rates of Qorg= 0.12 and 0.6 sccm lead to □pinene concentrations of 2 and 10 x1012 cm-3, respectively.

We are not aware of a suitable reference experiment with which to calibrate the SOA yield for αpinene ozonolysis. Yet a yield can be estimated with the model if [SOA] can be estimated from the observed growth. We illustrate this for one point in Fig. 7 where the experimental change in diameter is 29 nm at $Q_{org}$ = 0.6 sccm. Applying Eq. 1, an average value for the on-axis [SOA] of $2.0 \times 10^{10}$ $cm^{-3}$ is calculated (assuming the material that explains the measured particle growth is characteristic of a dimer.) Then we compare this to the average value of the ozone reaction placeholder in the model (without NOx' and photolysis shut off) with the flow entering the reactor containing 230 ppb ozone and 400 ppb αpinene. The ozone reaction placeholder has only loss to the wall as NO is absent and it attains an average on-axis concentration of $8.6 \times 10^{10}$ $cm^{-3}$ (using a diffusion coefficient of 0.045 atm $cm^2$ $s^{-1}$, which is characteristic of a dimer-type species). This results in an estimated yield of 0.23 which we consider uncertain to about 60 % primarily because we have no growth reference in this chemical system but also because the ozone instrument has not been calibrated recently.

However, this yield does not apply to αpinene ozonolysis alone as an OH scavenger was not present: the OH generated in the ozonolysis of αpinene leads to products that contribute to particle growth. There may be synergistic effects in the oxidation of αpinene when $O_3$ and OH are present[59]. The model, with $50^{40}$-$85^{70}$ % OH yield from the ozonolysis channel, indicates that OH addition pathways can contribute significantly to the observed 29 nm diameter increase. This is because without NO present the peroxy radicals can build to fairly high levels, allowing for significant dimerization and H-shifts for the peroxies. At an 85 % OH yield from αpinene ozonolysis, for example, the model-calculated LOP dimer is abundant enough to grow particles by 25 nm for these conditions (for the $RO_2$-R'$O_2$ rates and yields of dimer we have assumed.) The HOP dimers are also predicted to contribute substantially: particles could increase in diameter by 11 nm. These sum to a larger diameter change than was observed which indicates that the dimerization chemistry we assumed is too efficient, most likely the LOPdimers. More extensive and targeted experiments (including OH scavenging) and a proper, detailed treatment of the αpinene ozonolysis chemistry in the model would help to put limits on these branching ratios and yields.

## DISCUSSION

Amongst the numerous studies that have looked at SOA formation from the photo-oxidation of αpinene, limonene or myrcene, in Table 3 we compare our results to those studies where the amount of monoterpene reacted is low and initial SOA yields are either directly reported or can be deduced from the growth plots.

An early study by Ng et al.[7] presented growth plots where SOA yields can be deduced at early times. Their figure 4 initial slopes give mass-based yields of 0.031, 0.22, and 0.16 for αpinene, limonene, and myrcene, respectively: assuming a molar mass of 210 g/mol for the SOA material, these are molar yields of 0.02, 0.14, and 0.10, respectively. These values are in decent agreement with our values of 0.04, 0.084 and 0.16, respectively, considering uncertainties. The correlation of SOA yields with the number of double bonds are not the same in these two studies. There are significant experimental differences outlined in the Table. The experiments of Ng et al.[7] reached ΔHC (amount of αpinene reacted) of 100 μg/$m^3$ in about 12 min while this occurs in our experiments with a residence time of a little over a minute for $Q_H$ = 30 sccm. Presuming that a higher rate of oxidation leads to higher product concentrations, higher yields in our experiments would be expected, even for first-generation products. However, at

$Q_H$=3 sccm, where oxidation rates are low, both myrcene and limonene yields are unchanged, suggesting oxidation rate is not a factor for these experimental conditions. The trend with double bonds in our results agree with the double bond conclusions of the Moller et al.[55] theoretical study.

McVay et al.[8] investigated SOA yields for αpinene photooxidation and their results range from close to zero to about 0.07 on a molar basis for the initial part of their data (up to αpinene losses of 100 μg/m$^3$.) They also report 0.08 yield for experiments at one tenth the [OH] abundance, and they conclude that oxidation rates do not matter at long times. This range overlaps our value of 0.04 despite significant differences in experimental details. Eddingsaas et al.[9] report an increasing yield with OH exposure and their lowest exposure data give an SOA yield of about 0.02 with $NO_x$ present and 0.06 without $NO_x$ present, bracketing our yield.

Zhao et al.[10] studied SOA formed at low photo-oxidation rates from αpinene and from limonene but without seed aerosol. They report initial molar SOA yields of 0.0016 and 0.013 for αpinene and limonene, respectively, these do not agree with our results. Friedman and Farmer[68] deployed very high [OH] concentrations and report very low initial yields for both αpinene and limonene: they also had no seed particles but even their αpinene experiments with seeds present had initial yields very low.

Mutzel et al.[12] conducted measurements where reacted αpinene was quite low and their OH (in the presence of 10 ppb NO) at 50 % RH SOA final yields (converted to molar) are 0.022 for αpinene and 0.14 for limonene which are in good agreement with our results. They used slightly acidic (pH 4) ammonium hydrogen sulfate seed particles. Earlier experimental results from this group[11] are consistent with yields of ~ 0.08 for both αpinene and limonene. Initial yields (short times) for three of the four experiments[11,12] were much lower than the final yields.

Another type of measurement investigated oxidation of the three monoterpenes studied here: mass spectrometer measurements[18-21] of highly-oxidized molecules (HOMs). Jokinen et al.[20] deduced that the OH reactions with αpinene, limonene and myrcene show very small molar yields for HOMs, less than 1 %. Similar measurements but at different conditions[21] report a HOM yield of 0.012 for αpinene photooxidation. This suggests that the species responsible for the SOA in our experiments, if they are HOMs, are difficult to quantify in these types of measurements. On the other hand, αpinene ozonolysis HOM yields reported by Ehn et al.[19] are more in-line with the ozonolysis SOA yields in the Table; they also report a substantial increase in HOM yield for limonene compared to αpinene.

*Potential growth species*

The model was used to probe the abundance of gas-phase products of sufficiently low volatility to see whether they could cause significant particle growth and its dependence on experimental conditions, specifically [HONO]. Shown in Figure 8a are a set of species plotted against [HONO]; concentrations were taken at the middle of the flow reactor, R=0 and Z=60 cm. The range of [HONO] is shown in cm$^{-3}$ which is for $Q_H$ ranging from 5 to 35 sccm. We focus on peroxy radicals and products of both the initial (low oxygen-content) and the high oxygen-content peroxy (HOP) radicals and the three or more functional group nitrates.

The early $R(OH)O_2$ radical concentrations do not increase linearly with [HONO] as seen in Fig. 8a for the most abundant, APINBO2[40]. Yet their concentrations raised to the second power are closer to linear and determine the homogeneous dimer formation rate: indeed the sum of all low oxygen-content peroxy (LOP) dimer concentrations is nearly linear with [HONO]. The concentrations of the $R(OH)(O_{1,2}H)NO_3$, produced from LOPs, also grow linearly with HONO level. The species that arise from the HOPs (HOPdimers, red + and HOPnitrates, red squares) flatten out as HONO increases.

Figure 8b shows the predicted change in seed particle diameter for uptake of both types of dimers and to a heterogeneous process for the $R(OH)O_2$ (LOPs) along with the experimental data for αpinene from Fig. 4. The predicted change is according to Eq 1 using the mid-flow reactor concentrations, a decent proxy for the on-axis average concentration along the flow reactor. A heterogenous reaction is posited for the $R(OH)O_2$ radicals and subsequent diameter change with [HONO] is shown as the black + symbols.

A heterogeneous reaction amongst the initial peroxy radicals on the particle surface or in its bulk could yield dimers or other accretion products. Assuming a surface reaction, the uptake efficiency depends on parameters such as the adsorption equilibrium constant *b'* and the first-order rate coefficient on the surface, $k_s = k^{II}_{sur}[LOP]_{sur}$ (ref. 56; $k^{II}_{sur}$ is a second-order rate coefficient, molecule cm$^2$ s$^{-1}$) and for demonstration purposes we speculate values for *b'* of 0.02 cm and $k^{II}_{sur}$ of 2x10$^{-3}$ cm$^2$ s$^{-1}$. The uptake coefficient γ for an $RO_2$ molecule would scale with the sum of $[RO_2]_{sur}$ with γ ranging from 0.16 to 0.33 as the sum of $[RO_2]$'s goes from 2-to-6x10$^9$ cm$^{-3}$. The reasoning behind these choices of parameters are detailed in the Supplement.

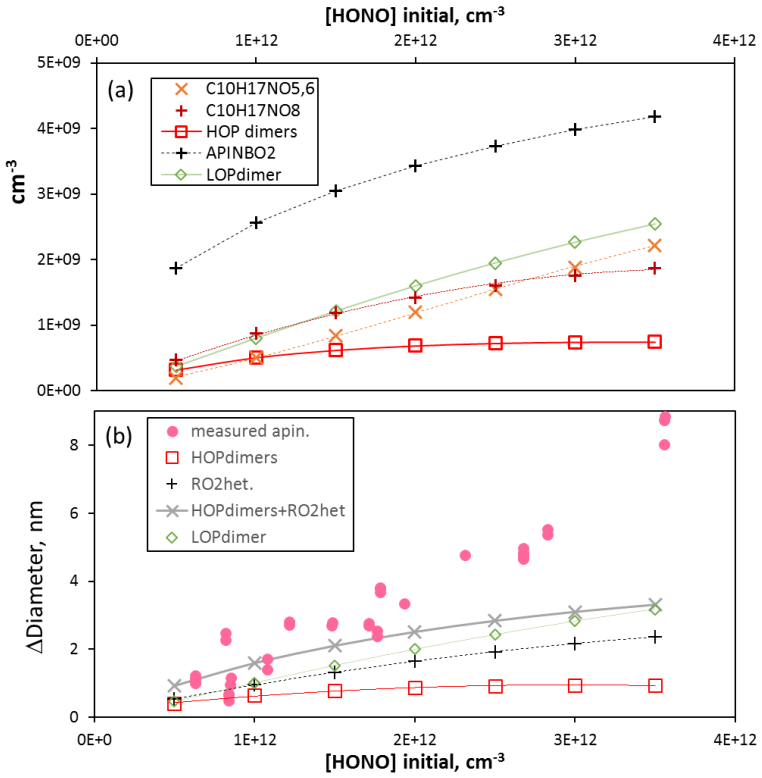


Figure 8. Model-calculations for αpinene photo-oxidation. The mid-flow reactor on-axis (r = 0, z = 60 cm) concentrations of (a) the most abundant initial peroxy radical, the sum of dimers formed from low oxygen-content peroxies (LOP dimers) and the sum of HOP dimers (formed from HOPs with 7 O atoms), and two sums of multifunctional nitrates. Panel (b) is a plot of the measured change in diameter of seed particles and that according to Eq 1 for the LOP and HOP dimers and a hypothesized heterogeneous reaction for LOPs. The range of HONO shown is for experimental $Q_H$ ranging from 5 to 35 sccm. Mid-flow reactor concentrations are within 20% of the concentrations averaged over the flow reactor length.

The sum of the model's HOP dimer and RO2het growth capabilities (grey + in Fig. 8a) is consistent with the measurements for the first half of the experimental range of HONO. The LOPdimers were not included in this sum as they are probably over-predicted in the model according to our ozone plus αpinene modeling discussed above. Representative species of a range of volatilities are listed in Table 2 along with their modeled pressures at a HONO level of $2x10^{12}$ $cm^{-3}$.

The least volatile species in the table are the multifunctional nitrates, $C_{10}H_{17}NO_{5,6}$ and $C_{10}H_{17}NO_8$. The nitrates from the HOPs ($C_{10}H_{17}NO_8$, taken to be 30% of the products from NO plus HOPs discussed above for Fig. 5) have four functional groups. The estimated equilibrium partitioning presented in Table 2 suggests dissolution into the organic layer of this HOP-derived nitrate could cause it to swell significantly. We note that there is a high level of uncertainty in the estimated saturation vapor pressures presented in Table 2 so a significant role for the LOP nitrates, $C_{10}H_{17}NO_{5,6}$, cannot be ruled out.

We think that slow accretion reactions between stable species that occur in the bulk of the particle[57,63] are probably not important for the present measurements although we have no experimental information on what species were taken up nor by what process. While particle-phase formation of sulfate esters and oligomerization etc. may take place, we estimate a very low value for an uptake coefficient for the abundant species, pinonaldehyde; see the Supplement for this and more discussion of particle-phase chemistry. While this chemistry can occur to some extent and it can be acid catalyzed by our seed particles, the presence of aqueous SA aerosol is not needed to grow particles: the growth observed in the nucleation measurements was 70 and 45 % of the growth onto SA seed particles for myrcene and limonene, respectively.

Differences in the limonene and myrcene photochemistry from that of αpinene that could explain the differences in the observed growth are probably in the H-shift rates for the different peroxy radicals formed upon OH addition. For example, myrcene has a number of allylic hydrogen atoms that are amenable to H-shift: Vereecken and Noziere[58] report H-shift rates of 2 $s^{-1}$ to 8 $s^{-1}$ that would apply to the myriad myrcene-$(OH)O_2$ species. See Tan et

al.[66] who present a detailed accounting of these species and potential H-shift rates based on the Vereecken and Noziere study. Our typical [NO] is $4x10^{10}$ $cm^{-3}$ and the pseudo-first order rate coefficient for myrcene-$(OH)O_2$ + NO is 0.4 $s^{-1}$ thus a dominant role for H-shift reactions that produce HOPs is likely for myrcene in our experiment. The peroxy radicals formed in limonene OH addition are similar to those formed in αpinene OH addition yet limonene has a high yield for the peroxy most likely to undergo H-shift: 37% for LIMCO2 (MCM designation[40], 39% in GECKO[65]) and ~22 % for APINCO2. Thus the increase in SOA formed from limonene over that formed from αpinene may be due to a more abundant HOP species. The further increase in SOA formation from myrcene might be explained in that a majority of the initial peroxy radicals[58] have significant H-shift rates, and these rates are likely greater than those for limonene and αpinene $RO_2$'s.

## CONCLUSIONS

The measured yield of the SOA products from photo-oxidation of these monoterpenes are found to be relatively constant with oxidation rate. But amongst the organic precursors, this yield increases with the number of double bonds in the initial compound, as noted in early experiments by Ng et al.[7] and recently in theoretical work by Moller et al.[58] The results of our experimental focus on first-generation products is consistent with the supposition that each additional double bond in these compounds leads to an approximately doubling in SOA yield going from αpinene to limonene to myrcene. Yet the trend within these monoterpenes is also that their structure becomes more open with the increase in the number of double bonds. More on how the structure influences SOA yields will be presented in a forthcoming paper (Sofio et al.[60]) that describes measurements for a wide range of organic species.

We have presented an experimental technique where particle growth can be studied with variable OH levels such that the OH exposure ([OH] times residence time) to oxidation products can be kept below $10^9$ molecule $cm^{-3}$ s. Our technique is akin to the oxidation flow reactor[61,29] but run under modest oxidation rates[62] and moderate NO levels. SOA yields were derived based on comparison to growth of seed particles due to $SO_2$ photo-oxidation. The method takes into account differences in wall loss rates and uses modeled OH production chain lengths to place $SO_2$ and monoterpene photo-oxidation on equal footing. The detailed branching ratios and yields from the model also highlight potential product species from αpinene that have behaviors and sufficient abundances to explain our observed particle growth.

The limonene SOA yields reported here compare well with previous results for similar amounts of reacted monoterpenes, while our αpinene results are in the midst of the scatter of the previous results. Our myrcene SOA yields are about double the only other report, the comprehensive Ng et al.[7] report. We also present particle nucleation from myrcene photo-oxidation that rivals and perhaps exceeds that from photo-oxidation of $SO_2$ at 35 % RH. The experimental results from photo-oxidation in our growth flow reactor are robust and in line with the results of other experiments. A forthcoming paper (Sofia et al. 2021[60]) presents the results from experiments designed to explore the dependence of SOA yield on the molecular structure of the organic precursor.

Overall, the formation of SOA material involves a combination of processes,[49,57,63] where involatile SOA species condense efficiently on particles, followed by dissolution of SOA species of a multitude of volatilities and then accretion reactions can occur between stable species. While the present experimental results cannot discern these pathways, the application of a kinetic model to the αpinene results has led to several insights. Involatile species initially taken up by particles are thought to be dimers formed in the gas-phase reactions of $RO_2$ radicals: we have proposed another source of involatile SOA species whereby $RO_2$ radicals react on surfaces forming dimers. A fast, heterogeneous reaction between $RO_2$ and adsorbed stable species may also play a role. The three and four functional group nitrates have sufficient abundances that more accurate estimates of their volatilities are needed to assess their contribution to the measured growth.

ACKNOWLEDGMENTS. We are grateful to J. Vences for initial testing of the instruments and the technique, A. Vang and S. Menheer for taking preliminary measurements and T. Kohls for exploring various strategies for implementing the chemical kinetics into the code. Conversations with J. Orlando are gratefully acknowledged. Research was funded by the NSF, grant AGS-1761638.

SUPPORTING INFORMATION. Detailed description of the αpinene chemistry and model results for a number of radical species in αpinene photooxidation and the radial distribution of $H_2SO_4$ as a growth agent. Also presented are experimental results for the NOx' measurements, growth as a function of (i) [$SO_2$], (ii) initial [αpinene] and (iii) without any organic compounds, and the size distributions for the thermodenuder experiments and for the nucleation results.

Table 1. Growth Flow Reactor Typical Conditions

| Exp. Conditions | | Typical levels | |
|---|---|---|---|
| P, T | 0.97 atm, 23 $^0$C | Organic | 300 ppbv |
| R.H. | 35 % | HONO | 42 ppbv |
| $Q_{total}$ | 1.55 sLpm | NO, $NO_2$ [b] | 1.5 ppbv |
| $V_{ave}$ | 1.5 cm/s | Seed $D_p$, $N_p$ | 8−10 nm, $3x10^3$ $cm^{-3}$ |
| $t_{res.}$ [e] | 85 s | $k_{part}$, $k_{wall}$ [c] | $3x10^{-5}$, 0.03 ($s^{-1}$) |
| $Q_H$ [a] | 0.005-0.035 sLpm | OH prod. rate [d] | $2x10^9$ $cm^{-3}$ $s^{-1}$ |

[a] Flow of HCl-laden air through NaONO vessel.
[b] Initial levels entering flow reactor with HONO.
[c] First-order loss rate coefficients to seed particles and to the wall, resp.
[d] Primary OH from HONO photolysis rate coeff. of $2x10^{-3}$ $s^{-1}$.
[e] Average residence time. On-axis residence time is half that.

Table 2. Estimated partitioning of semivolatile species. Modeled partial pressure at $Q_H$=20 sccm, saturation pressure, mole fraction in the organic layer.

| Species | $P_{model}$ (atm) | $P_{sat}$[a] (atm) | $x_{org}$ [b] |
|---|---|---|---|
| Pinonaldehyde | $2x10^{-9}$ | $4x10^{-6, 69}$ | 0.0005 |
| APINBNO3 | $2x10^{-10}$ | $1.3x10^{-6, 67}$ | 0.0002 |
| 8-OOH-en-6-one | $2x10^{-10}$ | $2.6x10^{-6, 67}$ | 0.0001 |
| R(OH)(OOH) | $1.6x10^{-10}$ | $4x10^{-8, 67}$ | 0.004 |
| $R(OH)(O_{1,2}H)(NO_3)$ | $2.5x10^{-11}$ | $6x10^{-10, 48}$ | 0.04 |
| $ROO(OH)(OOH)(NO_3)$[c] | $6x10^{-11}$ | $1.6x10^{-10, 48}$ | 0.4 |

[a.] From refs. 67, 48 (SIM method) or 69 (COSMOTHERM).
[b.] From $x_{org} = P_{model}/(\gamma P_{sat})$ assuming activity coefficient $\gamma$ is unity. Molarities in the $H_2O/H_2SO_4$ seed are less than $1x10^{-3}$ M (assuming aqueous 15 °C Henry's Law solubilities[69]; conjugates used for 3rd and 5th and 6th entries) except for the 6th entry, $6x10^{-3}$ M.
[c.] Assuming –OO– bridge is equivalent to a carbonyl group.

Table 3. Molar SOA yields, limited to small amounts of reacted monoterpene: < 100 μg/m$^3$.

| Ref., chamber vol. (FR:flow reactor) | Oxidant (and source) | [OH], $10^6$cm$^{-3}$ | $NO_x$, ppb | RH | Initial MT ppb | time [g] min | Seeds [e] | SOA yield (* from HOM) αpinene | limonene | myrcene |
|---|---|---|---|---|---|---|---|---|---|---|
| Ng [7], 28 m$^3$ | OH (HONO 354 nm) | 7 [h] | ~100 | 45 | 108 | 40 | AS | 0.025 | 0.14 | 0.10 |
| McVay[8], 24 m$^3$ | OH ($H_2O_2$ UVA) | 2 | < 2 | < 5 | 50 | 40, 70[#] | AS | 0.02,0.07[#] | - | - |
| " | " | 0.2 | " | < 5 | 50 | 160 | AS | 0.08 | - | - |
| Eddingsaas[9], 28 m$^3$ | OH ($H_2O_2$) | 2 | - | < 10 | 50 | 18 | AS | 0.06 [a] | - | - |
| " | (HONO/ $CH_3ONO$) | 6-20 | 100s | < 10 | 50 | 13 | AS | 0.02 [a] | - | - |
| Zhao [10], 270 m$^3$ | OH (HONO, sun) | 6.4 | < 1 | ~ 60 | 4 | 55, 15[#] | None | 0.0016 | 0.013[#] | - |
| Friedman[68], FR | OH ($O_3$, 254 nm) | 50000 | - | 0 | 20-300 | 2 | None | 0.0005 | 0.001 | - |
| Mutzel [11], 19 m$^3$ | OH ($H_2O_2$ 254 nm) | - | < 1 | 50 | 25 | 20 | AHS | 0.08 | 0.08 [d] | - |
| Mutzel [12], 19 m$^3$ | OH ($H_2O_2$ UVA) | 4 | 10 | 50 | 60 | 90 | AS/SA | 0.022 [d] | 0.14 [d] | - |
| **this work[b], FR** | OH (HONO 367 nm) | 0.3-20 [f] | 2 to 10 | 35 | 200-400 | 1.3 | SA | **0.040** | **0.084** | **0.16** |
| Jokinen [20], FR | OH | - | - | 25 | 0.04-400 | 0.7 | n/a | 0.0044 * | 0.0093 * | 0.01 * |
| Kirkby [21], 26 m$^3$ | OH | 0.1 | - | 38 | 0.1-2 | - | n/a | 0.012 * | - | - |
| | | [$O_3$] ppb | | | | | | | | |
| Jokinen [20], FR | $O_3$ | 25 | | 25 | 0.04-400 | 0.7 | n/a | 0.034 * | 0.053 * | 0.0047 * |
| Kirkby [21], 26 m$^3$ | $O_3$ | 20-40 | | 38 | 0.1-2 | - | n/a | 0.029 * | - | - |
| Ehn [19], 1.5 m$^3$ | $O_3$ / OH | 12-86 | | 63 | 0-30 | 45 | n/a | 0.07 * | 0.17 * | - |
| Krasnomowitz[13], FR | $O_3$ | 30-250 | | 10 | 11 | 8 | AS | 0.13 | - | - |
| Burkholder[14], 70 L | $O_3$ / OH | 0.1-4000 | | 0 | 0.6-50 | 17 | None | 0.06 | - | - |
| Ng [7], 28 m$^3$ | $O_3$ | 550 | | <10 | 185 | 40 | AS | 0.10 | - | 0.016 |
| **this work[c], FR** | $O_3$ / OH | 230 | | 35 | 80-400 | 1.3 | SA | **0.23** | - | - |

Where mass-based SOA yields are reported in previous work, a molar mass of 210 g/mol was assumed for the SOA material, as it was done for the present work along with a density of 1.2 g/cm$^3$.

[a] Average of the first few [OH]*time data points.

[b] Yields based on comparison to growth via $H_2SO_4$ in conjunction with modeled photochemistry. Uncertainty is ±40 %.

[c] Yield based only on modeled ozonolysis of αpinene. Uncertainty is ±60%.

[d.] Very little SOA was formed in the initial phases of photooxidation.

[e.] AS = $(NH_4)_2SO_4$, AHS = $(NH_4)HSO_4$, SA = $H_2O/H_2SO_4$

[f.] Model-calculated. Lowest [OH] for αpinene: 4x10$^6$, limonene: 2x10$^6$, and myrcene: 3x10$^5$.

[g.] MT, monoterpene. Estimated time along growth curve that yield was determined.

[h.] Estimated from αpinene decay.

REFERENCES


1. Jimenez, J. L.; Canagaratna, M. R.; Donahue, N. M.; Prevot, A. S. H.; Zhang, Q.; Kroll, J. H.; DeCarlo, P. F.; Allan, J. D.; Coe, H.; Ng, N. L.; et al.: Evolution of organic aerosols in the atmosphere, *Science*, 326, **2009**, 1525–1529.
2. Kroll, J. H.; Seinfeld, J. H. Chemistry of secondary organic aerosol: Formation and evolution of low-volatility organics in the atmosphere. *Atmos. Environ.* **2008**, 42, 3593−3624.
3. Hallquist, M.; Wenger, J. C.; Baltensperger, U.; Rudich, Y.; Simpson, D.; Claeys, M.; Dommen, J.; Donahue, N. M.; George, C.; et al. The formation, properties and impact of secondary organic aerosol: current and emerging issues. *Atmos. Chem. Phys.* **2009**, 9, 5155−5236.
4. Ziemann, P. J.; Atkinson, R. Kinetics, products, and mechanisms of secondary organic aerosol formation. *Chem. Soc. Rev.* **2012,** 41, 6582–605.
5. Lee, A.; Goldstein, A. H.; Keywood, M. D.; Gao, S.; Varutbangkul, V.; Bahreini, R.; Ng, N. L.; Flagan, R. C.; Seinfeld, J. H. Gas-phase products and secondary aerosol yields from the ozonolysis of ten different terpenes. *J. Geophys. Res. Atmos.* **2006,** *111*(7). https://doi.org/10.1029/2005JD006437

6. Lee, A.; Goldstein, A. H.; Kroll, J. H.; Ng, N. L.; Varutbangkul, V.; Flagan, R. C.; Seinfeld, J. H. Gas-phase products and secondary aerosol yields from the photooxidation of 16 different terpenes. *J.Geophys. Res. Atmos.* 2006, *111*(17). https://doi.org/10.1029/2006JD007050
7. Ng, N. L.; Kroll, J. H.; Keywood, M. D.; Bahreini, R.; Varutbangkul, V.; Flagan, R. C.; Seinfeld, J. H.; Lee, A.; Goldstein, A. H. Contribution of first- versus second-generation products to secondary organic aerosols formed in the oxidation of biogenic hydrocarbons. *Envir. Sci. Tech.* **2006** *40*(7), 2283–2297.
8. McVay, R. C.; Zhang, X.; Aumont, B.; Valorso, R.; Camredon, M.; La, Y. S.; Wennberg, P. O.; Seinfeld, J. H. SOA formation from the photooxidation of α-pinene: systematic exploration of the simulation of chamber data, *Atmos. Chem. Phys.* **2016**, 16, 2785–2802.
9. Eddingsaas, N. C.; Loza, C. L.; Yee, L. D.; Chan, M.; Schilling, K. A.; Chhabra, P. S.; Seinfeld, J. H.; Wennberg, P. O. α-pinene photooxidation under controlled chemical conditions-Part 2: SOA yield and composition in low-and high-NO x environments. *Atmos. Chem. Phys.* **2021**, *12*(16), 7413–7427.
10. Zhao, D. F.; Kaminski, M.; Schlag, P.; Fuchs, H.; Acir, I.-H.; Bohn, B.; Häseler, R.; Kiendler-Scharr, A.; Rohrer, F.; Tillmann, R.; et al. Secondary organic aerosol formation from hydroxyl radical oxidation and ozonolysis of monoterpenes, *Atmos. Chem. Phys.*, **2015** 15, 991–1012.
11. Mutzel, A.; Rodigast, M.; Iinuma, Y.; Böge, O.; Herrmann, H. Monoterpene SOA - Contribution of first-generation oxidation products to formation and chemical composition. *Atmospheric Environment* **2016**, *130*, 136–144.
12. Mutzel, A.; Zhang, Y.; Böge, O.; Rodigast, M.; Kolodziejczyk, A.; Wang, X.; Herrmann, H. Importance of secondary organic aerosol formation of α-pinene, limonene, and m-cresol comparing day- And nighttime radical chemistry. *Atmos. Chem. Phys.* **2021,** *21*(11), 8479–8498.
13. Krasnomowitz, J. M.; Apsokardu, M. J.; Stangl, C. M.; Tiszenkel, L.; Ouyang, Q.; Lee, S.; Johnston, M. V. Growth of Aitken mode ammonium sulfate particles by α-pinene ozonolysis. *Aeros. Sci. Tech.* **2019,** *53*(4), 406–418.
14. Burkholder, J.B.; Baynard,T.; Ravishankara,A.R.; Lovejoy, E.R Particle nucleation following the O3 and OH initiated oxidation of a-pinene and b-pinene between 278 and 320K. *J. Geophys. Res.* **2007**, 112, D10216.
15. Donahue, N. M.; Epstein, S. A.; Pandis, S. N.; Robinson, A. L. A two-dimensional volatility basis set: 1. organic-aerosol mixing thermodynamics. *Atmos. Chem. Phys.* **2011,** 11, 3303–3318.
16. Cappa, C. D.; Wilson, K. R. Multi-generation gas-phase oxidation, equilibrium partitioning, and the formation and evolution of secondary organic aerosol. *Atmos. Chem. Phys.* **2012**, 12, 9505–9528.
17. Donahue, N. M.; Robinson, A. L.; Trump, E. R.; Riipinen, I.; Kroll, J. H. (2012). *Volatility and Aging of Atmospheric Organic Aerosol* (pp. 97–143), Ed. V. F. McNeill, P. A. Ariya. Springer, Berlin, Heidelberg.
18. Zhao, J.; Ortega, J.; Chen, M.; McMurry, P. H.; Smith, J. N. Dependence of particle nucleation and growth on high-molecular-weight gas-phase products during ozonolysis of α-pinene. *Atmos. Chem. Phys*. **2013**, *13*(15), 7631–7644.
19. Ehn, M.; Thornton, J. A.; Kleist, E.; Sipilä, M.; Junninen, H.; Pullinen, I.; Springer, M.; Rubach, F.; Tillmann, R.; Lee, B.; et al. A large source of low-volatility secondary organic aerosol. *Nature* **2014**, *506*(7489), 476–479.
20. Jokinen; T.; Berndt, T.; Makkonen; R.; Kerminen, V.-M.; Junninen; H.; Paasonen, P.; Stratmann; F.; Herrmann, H.; Guenther; A. B.; et al. Production of extremely low volatile organic compounds from biogenic emissions: Measured yields and atmospheric implications. *Proc. Natl. Acad. Sci. U. S. A.* **2015**, 112, 7123−7128.
21. Kirkby, J.; Duplissy, J.; Sengupta, K.; Frege, C.; Gordon, H.; Williamson, C.; Heinritzi, M.; Simon, M.; Yan, C.; et al. Ion-induced nucleation of pure biogenic particles. *Nature* **2016**, 533, 521−524.
22. Crounse, J. D.; Nielsen, L. B.; Jørgensen, S.; Kjaergaard, H. G.; Wennberg, P. O. Autoxidation of organic compounds in the atmosphere. *J. Phys. Chem. Lett*. **2013**, *4*(20), 3513–3520.
23. Berndt, T.; Scholz, W.; Mentler, B.; Fischer, L.; Herrmann, H.; Kulmala, M.; Hansel, A. Accretion product formation from self- and cross-reactions of RO2 radicals in the atmosphere. *Angewandte Chemie - International Edition*, **2018**, *57*(14), 3820–3824.
24. Zhao, Y.; Thornton, J. A.; Pye, H. O. T. Quantitative constraints on autoxidation and dimer formation from direct probing of monoterpene-derived peroxy radical chemistry. *Proc. Natl. Acad. Sci. U. S. A.* **2018**, *115*(48), 12142–12147.
25. Xu, L.; Møller, K. H.; Crounse, J. D.; Otkjær, R. v.; Kjaergaard, H. G.; Wennberg, P. O. Unimolecular reactions of peroxy radicals formed in the oxidation of α-Pinene and β-Pinene by hydroxyl radicals. *J. Phys. Chem. A*, **2019**, *123*(8), 1661–1674.

26. Bianchi, F.; Kurtén, T.; Riva, M.; Mohr, C.; Rissanen, M. P.; Roldin, P.; Berndt, T.; Crounse, J. D.; Wennberg, P. O.; Mentel, T. F.; Wildt, J.; Junninen, H. Highly oxygenated organic molecules (HOM) from gas-phase autoxidation involving peroxy radicals: A key contributor to atmospheric aerosol. *Chem. Rev.* **2019**, 119, 3472–3509.
27. Hanson, D. R.; Abdullahi, H.; Menheer, S.; Vences, J.; Alves, M. R.; Kunz, J. H2SO4 and particle production in a photolytic flow reactor: chemical modeling, cluster thermodynamics and contamination issues, *Atmos. Chem. Phys.* **2019**, 19, 8999–9015.
28. Hanson, D. R.; Menheer, S.; Wentzel, M.; Kunz, J. Measurement report: Sulfuric acid nucleation and experimental conditions in a photolytic flow reactor. *Atmos. Chem. Phys*. **2021**, *21*(3) unh .
29. Lambe, A. T.; Onasch, T. B.; Croasdale, D. R.; Wright, J. P.; Martin, A. T.; Franklin, J. P.; Massoli, P.; Kroll, J. H.; Canagaratna, M. R.; Brune,W. H.; et al. Transitions from functionalization to fragmentation reactions of laboratory secondary organic aerosol (SOA) generated from the OH oxidation of alkane precursors, *Environ. Sci. Technol.* **2012**, 46, 5430–5437.
30. Jiang, J.; Chen, M.; Kuang, C.; Attoui, M.; McMurry, P. H. Electrical mobility spectrometer using a diethylene glycol condensation particle counter for measurement of aerosol size distributions down to 1 nm. *Aeros. Sci. Tech.* **2011**, 45(4), 510–521.
31. Kuang, C.; Chen, M.; McMurry, P. H.; Wang, J. Modification of laminar flow ultrafine condensation particle counters for the enhanced detection of 1 nm condensation nuclei, *Aerosol Sci. Tech.* **2012**, 46, 309–315.
32. Wexler, A. S.; Clegg, S. L. Atmospheric aerosol models for systems including the ions H+, NH4+, Na+, $SO_4^{2-}$, $NO_3^-$, Cl-, Br-, and $H_2O$, *J. Geophys. Res.* **2002**, 107, 4207.
33. Lovejoy, E. R.; Curtius, J.; Froyd, K. D Atmospheric ion induced nucleation of sulfuric acid and water, *J. Geophys. Res.* **2004**, 109, D08204.
34. Febo, A.; Perrino, C.; Sparapani, R.; Gherardi, M. Evaluation of a high-purity and high-stability continuous generation system for nitrous acid, *Environ. Sci. Technol.* **1995**, 29, 2390–2395.
35. Gingerysty, N. J.; Osthoff, H. D. A compact, high-purity source of HONO validated by Fourier transform infrared and thermal-dissociation cavity ring-down spectroscopy, *Atmos. Meas. Tech.* **2020**, 13, 4159–4167.
36. P.J. Linstrom and W.G. Mallard, Eds., NIST Chemistry WebBook, NIST Standard Reference Database Number 69, National Institute of Standards and Technology, Gaithersburg MD, 20899, https://doi.org/10.18434/T4D303, (retrieved September 22, 2021).
37. Hawkins, J.E.; Armstrong, G.T. Physical and thermodynamic properties of terpenes. III. The vapor pressures of α-pinene and β-pinene, *J. Am. Chem. Soc,* **1954**, 76, 14, 3756-3759.
38. Stull, D. R. Vapor pressures of pure substances. Organic and inorganic compounds, *Ind. Eng. Chem.* **1947**, 39, 4, 517-540.
39. Vereecken, L.; Müller, J. F.; Peeters, J. Low-volatility poly-oxygenates in the OH-initiated atmospheric oxidation of α-pinene: Impact of non-traditional peroxyl radical chemistry *Phys. Chem. Chem. Phys.* **2007**, *9*(38), 5241–5248.
40. Saunders, S. M.; Jenkin, M. E.; Derwent, R. G.; Pilling, M. J. Protocol for the development of the Master Chemical Mechanism, MCMv3 (Part A): tropospheric degradation of non-aromatic volatile organic compounds. *Atmos. Chem. Phys.* **2003**, 3, 161–180.
41. Verheggen, B.; Mozurkewich, M. Determination of nucleation and growth rates from observation of a SO2 induced atmospheric nucleation event *J. Geophys. Res.* **2002**, 107, 4123.
42. Lehtinen, K. E. J.; Kulmala, M. A model for particle formation and growth in the atmosphere with molecular resolution in size, *Atmos. Chem. Phys.* **2003**, 3, 251–257.
43. Stolzenburg, D.; Simon, M.; Ranjithkumar, A.; Kürten, A.; Lehtipalo, K.; Gordon, H.; Ehrhart, S.; Finkenzeller, H.; Pichelstorfer, L.; Nieminen, T.; et al. Enhanced growth rate of atmospheric particles from sulfuric acid, Atmos. Chem. Phys. **2020**, 20, 7359–7372.
44. Hanson, D. Mass accommodation of $H_2SO_4$ and $CH_3SO_3H$ on water-sulfuric acid solutions from 6 to 97% RH *J. Phys. Chem. A* **2005**, 109, 6919–6927.
45. Hanson, D. R.; Eisele, F. Diffusion of $H_2SO_4$ in humidified nitrogen: Hydrated $H_2SO_4$. *J. Phys. Chem. A* **2000**, *104*, 1715-1719.
46. Reid, R.C.; Prausnitz, J. M.; Sherwood, T. K., Ch. 11 Diffusion Coefficients, in *The Properties of Gases and Liquids*,3rd ed.; McGraw-Hill, 1977; p 554.
47. Hanson, D.; Orlando, J.; Noziere, B.; Kosciuch, E Proton transfer mass spectrometry studies of peroxy radicals. *Int. J. Mass Spec.* **2004**, *239*, 147–159.

48. Valorso, R.; Aumont, B.; Camredon, M.; Raventos-Duran, T.; Mouchel-Vallon, C.; Ng, N. L.; Seinfeld, J. H.; Lee-Taylor, J.; Madronich, S. Explicit modelling of SOA formation from $\alpha$-pinene photooxidation: sensitivity to vapour pressure estimation, *Atmos. Chem. Phys.* **2011**, 11, 6895–6910.
49. Schervish, M.; Donahue, N. M. Peroxy radical chemistry and the volatility basis set. *Atmos. Chem. Phys.* **2020**, *20*, 1183–1199.
50. Berndt, T.; Richters, S.; Jokinen, T.; Hyttinen, N.; Kurten, T.; Otkjaer, R. V.; Kjaergaard, H. G.; Stratmann, F.; Herrmann, H.; Sipilä, M.; Kulmala, M.; Ehn, M. Hydroxyl radical-induced formation of highly oxidized organic compounds. *Nat. Commun.* **2016**, 7, 13677.
51. Cain, K.P.; Karnezi, E.; Pandis, S. N. Challenges in determining atmospheric organic aerosol volatility distributions using thermal evaporation techniques, *Aerosol Sci. Tech.* **2020**, 54:8, 941-957.
52. Zhao, Z.; Yang, X.; Lee, J.; Tolentino, R.; Mayorga, R.; Zhang, W.; Zhang, H. Diverse reactions in highly functionalized organic aerosols during thermal desorption. *ACS Earth Space Chem.* **2020**, 4 (2), 283−296.
53. Ayers, G.P.; Gillett, R.W.; Gras, J. L. On the vapor pressure of sulfuric acid, *Geophys. Res. Lett.* **1980**, 7, 433-436.
54. Gmitro, J. T.; Vermeulen, T. Vapor–liquid equilibria for aqueous sulfuric acid, *AIChE J.* **1964**, 10, 740–746.
55. Møller, K.H.; Otkjær, R.V., Chen, J.; Kjaergaard, H. G. Double bonds are key to fast unimolecular reactivity in first-generation monoterpene hydroxy peroxy radicals, *J. Phys. Chem. A* **2020** *124*, 2885-2896.
56. Hanson, D. R. Surface-specific reactions on liquids. *J. Phys. Chem. B* **1997**, *101*, 4998-5001.
57. Apsokardu, M. J.; Johnston, M. V. Nanoparticle growth by particle-phase chemistry. *Atmos. Chem. Phys.* **2018**, 18 (3), 1895–1907.
58. Vereecken, L.; Nozière, B. H migration in peroxy radicals under atmospheric conditions. *Atmos. Chem. Phys.* **2020**, *20*(12), 7429–7458.
59. Kenseth C. M.; Huang, Y.; Zhao, R.; Dalleskab, N. F.; Hethcox, J. C.; Stoltz, B. M.; Seinfeld J. H. Synergistic O3 + OH oxidation pathway to extremely low-volatility dimers revealed in β-pinene secondary organic aerosol. *Proc. Nat. Acad. Sci. USA* **2018**, 115, 8301–8306.
60. Sofio et al., in preparation.
61. Peng, Z.; Day, D. A.; Stark, H.; Li, R.; Lee-Taylor, J.; Palm, B. B.; Brune, W. H.; and Jimenez, J. L. HOx radical chemistry in oxidation flow reactors with low-pressure mercury lamps systematically examined by modeling *Atmos. Meas. Tech.* **2015**, 8, 4863–4890.
62. Lambe, A. T.; Krechmer, J. E.; Peng, Z.; Casar, J. R.; Carrasquillo, A. J.; Raff, J. D.; Jimenez, J. L.; Worsnop, D. R. $HO_x$ and $NO_x$ production in oxidation flow reactors via photolysis of isopropyl nitrite, isopropyl nitrite-$d_7$, and 1,3-propyl dinitrite at $\lambda = 254$, 350, and 369 nm, *Atmos. Meas. Tech.* **2019**, 12, 299–311.
63. Barsanti, K. C.; Kroll, J. H.; Thornton, J. A. Formation of low-volatility organic compounds in the atmosphere: Recent advancements and insights. *J. Phys. Chem. Lett.* **2017**, 8, 1503−1511.
64. Pagonis, D.; Ziemann, P.J. Chemistry of hydroperoxycarbonyls in secondary organic aerosol, *Aerosol Sci. Tech.* **2018**, 52, 1178-1193.
65. Afreh, I. K.; Aumont, B.; Camredon, M.; Barsanti, K. C. Using GECKO-A to derive mechanistic understanding of SOA formation from the ubiquitous but understudied camphene, *Atmos. Chem. Phys.* **2020**, 21, 11467–11487.
66. Tan, Z.; Hantschke, L.; Kaminski, M.; Acir, I.-H.; Bohn, B.; Cho, C.; Dorn, H.-P.; Li, X.; Novelli, A.; Nehr, S. Atmospheric photo-oxidation of myrcene: OH reaction rate constant, gas-phase oxidation products and radical budgets, *Atmos. Chem. Phys.* **2021**, 21, 16067–16091.
67. Capouet, M.; Muller, J.-F. A group contribution method for estimating the vapour pressures of a-pinene oxidation products, *Atmos. Chem. Phys.* **2006**, 6, 1455–1467.
68. Friedman, B.; Farmer, D.K. SOA and gas phase organic yields from the sequential photooxidation of seven monoterpenes, *Atmos. Environ.* **2018**, 187, 335–345.
69. Wang, C.; Yuan, T.; Wood, S. A.; Goss, K.-U.; Li, J.; Ying, Q.; Wania, F. Uncertain Henry's law constants compromise equilibrium partitioning calculations of atmospheric oxidation products, *Atmos. Chem. Phys.* **2017**, 17, 7529–7540.
70. Atkinson, R.; Arey, J. Atmospheric degradation of volatile organic compounds, *Chem. Rev.* **2003**, 103, 4605-4638